Electron paramagnetic resonance determination of the local field distribution acting on Cr^{3+} and Fe^{3+} in transition metal fluoride glasses (TMFG)

1995 J. Phys.: Condens. Matter 7 3853

(http://iopscience.iop.org/0953-8984/7/20/006)

J. Phys.: Condens. Matter 7 (1995) 3853–3862. Printed in the UK

Electron paramagnetic resonance determination of the local field distribution acting on Cr^{3+} and Fe^{3+} in transition metal fluoride glasses (TMFG)

C Legein†, J Y Buzaré‡, J Emery‡ and C Jacoboni†

† Laboratoire des Fluorures, URA CNRS 449, Faculté des Sciences, Université du Maine, 72017 Le Mans Cédex, France

‡ Equipe de Physique de l'Etat Condensé, URA CNRS 807, Faculté des Sciences, Université du Maine, 72017 Le Mans Cédex, France

Received 13 October 1994, in final form 6 February 1995

Abstract. Cr^{3+} and Fe^{3+} ions are used as paramagnetic probes of the local order in diamagnetic transition metal fluoride glasses (TMFG). EPR observations are made at S, X, K and Q band frequencies at different temperatures. It follows from the frequency dependence of the spectra that Cr^{3+} and Fe^{3+} ions are characterized by a continuous fine-structure parameter distribution in the range 0.06–0.55 cm^{-1} for Cr^{3+} and 0.04–0.33 cm^{-1} for Fe^{3+}. The simulations of these spectra are computed with a fine-structure parameter distribution $P(b_2^0, \lambda)$ whose expression is determined by analogy with the distribution of electric field gradient $P(V_{zz}, \eta)$ developed by Czjzek considering amorphous solids with random ionic coordination. An excellent agreement between observed and calculated spectra is obtained whatever the frequency band.

1. Introduction

Most experimental data on degree of short range ordering in disordered solids are traditionally obtained using diffraction techniques and EXAFS. They yield information on the number and radial distances of atoms in the first coordination shells but give no information on their angular distribution. Other experimental techniques able to investigate angular atomic coordination are highly desirable.

One possibility is provided by electron paramagnetic resonance (EPR) which is well known to supply valuable information about the local site symmetries, but, in order to make EPR an efficient tool for structural investigation of disordered materials, two problems have to be solved. The first one is the formalism used to explain the EPR spectra; the second one concerns the parametrization of the spectra in order to extract a description of the short-range ordering.

The present paper deals with an attempt to answer the first question within the frame of transition metal fluoride glasses (TMFG). In a forthcoming paper, local structure modelling will be presented that characterizes the local short-range order around the EPR probes.

Previous structural studies in various fields have shown that the TMFG network is built up from corner-shared $M^{II}F_6$ and $M^{III}F_6$ octahedra [1, 2]. In these glasses, 3d transition metal ions, which are well known to adopt octahedral coordination in a fluoride medium, can be used as true local EPR probes. In a previous paper [3], we have presented the results of an EPR study of TMFG separately doped with Ti^{3+}, Cr^{3+}, Fe^{3+}, Mn^{2+}, Co^{2+} and Cu^{2+}

0953-8984/95/203853+10$19.50

ions. In this paper, we focused our EPR study on Cr^{3+} and Fe^{3+} ions whose fine-structure parameters are very sensitive to local structure.

The aim of this paper is to obtain information on local field symmetry through computed reconstruction of EPR spectra. Computing of EPR spectra is achieved through different stages: a frequency study firstly allowed us to estimate Cr^{3+} and Fe^{3+} fine-structure parameter values in TMFG. The distribution of these parameters has been determined from EPR spectra reconstruction by using the Czjzek distribution function [4]; in the second part of this paper we will justify this choice and present the computer procedure and finally the calculated spectra.

2. Experimental procedures

EPR spectra were studied on TMFG derived from two base glasses: PZG (35 PbF_2, 24 ZnF_2, 34 GaF_3, 5 YF_3, 2 AlF_3 (mol%)) [5] and PBI (19 PbF_2, 23 BaF_2, 47 InF_3, 2 AlF_3, 4.5 YF_3, 4.5 SrF_2 (mol%)) [6]. CrF_3 and FeF_3 were added at different concentrations. After preliminary mixing, the melt was placed in covered platinum crucible and heated at 800 °C, and then cast into a preheated (200 °C) mould.

The X band (9.5 GHz) and S band (4 GHz) spectra were recorded on a Bruker spectrometer; measurements at variable temperature (X band) were achieved by using an Oxford cryostat. The K band spectrometer (19 GHz) was designed and assembled in IBM Zurich [7]. Q band spectra (35 GHz) were recorded by P Simon in the CRPHT (UP CNRS 4212).

3. The frequency dependence study of Cr^{3+} and Fe^{3+} EPR spectra: the estimation of fine-structure parameters

3.1. Temperature and concentration dependence

In a previous work [3], we studied the effect of temperature and doping concentration on EPR spectra of TMFG:Cr^{3+} and Fe^{3+}. In both cases, the marked changes imply the presence of more than one paramagnetic species in the glasses. The observed spectra were attributed to a combination of isolated paramagnetic ions and exchange coupled pairs.

This is why, as far as possible, we have recorded Cr^{3+} and Fe^{3+} EPR spectra at low temperature for samples with low Cr^{3+} or Fe^{3+} doping concentration. Thus, Cr^{3+} and Fe^{3+} spectra can be attributed to isolated ions. Nevertheless, for S and Q bands, operation at liquid helium temperature could not be achieved. This is of no consequence because for both these microwave frequencies Cr^{3+} and Fe^{3+} EPR spectra exhibit a single broad resonance (see subsection 3.2).

3.2. Results

The dependence of the Cr^{3+} EPR spectra on the microwave frequency is shown in figure 1.

(i) At the S band (figure 1(a)), the spectrum is dominated by a low-field resonance with $g_{\text{eff}} = 5.0$ ($g_{\text{eff}} = h\nu/\beta H$ with H the magnetic field value where the EPR spectra reduce to zero for the Fe^{3+} resonances and the Cr^{3+} $g_{\text{eff}} = 1.97$ resonance; for the Cr^{3+} $g_{\text{eff}} = 5.0$ resonance, the H value is taken to the maximum).

(ii) The X band spectrum exhibits two broad resonances at $g_{\text{eff}} = 5.0$ and $g_{\text{eff}} = 1.97$ (figure 1(b)). A narrow resonance is observed near zero field at low temperature and concentration ($T < 20$ K, $c \leqslant 0.50$ wt% CrF_3).

(iii) At the K band, the absorption in the $g_{eff} = 1.97$ region has developed into a well defined broad resonance when the intensity (peak to peak height X (HWHM)^2 for derivative spectrum) of the signal at $g_{eff} = 5.0$ is reduced (figure 1(c)); one resonance near zero field is observed at low temperature ($T < 10$ K, $c \leqslant 0.50$ wt% CrF_3).

(iv) At the Q band (figure 1(d)), the $g_{eff} = 5.0$ resonance is nearly suppressed; the $g_{eff} = 1.97$ feature becomes the most prominent.

A similar frequency effect is evident in Fe^{3+} EPR spectra as shown in figure 2. When the microwave frequency increases an enhancement of the intensity of the $g_{eff} = 2.0$ resonance is observed when the intensity of the $g_{eff} = 4.3$ resonance decreases. A narrow resonance is also observed near zero field in X ($T < 20$ K, $c < 0.50$ wt% FeF_3) and K ($T < 10$ K, $c < 0.50$ wt% FeF_3) band spectra.

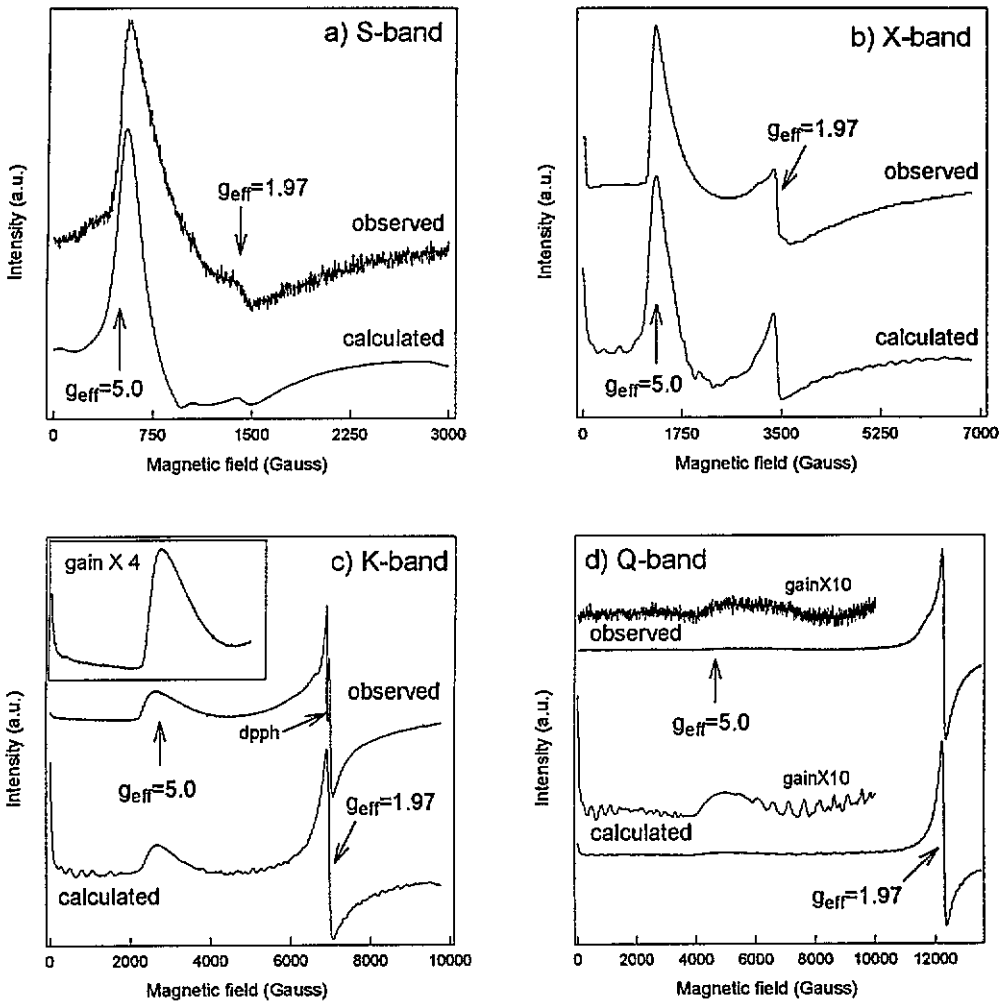

Figure 1. Observed and calculated EPR Cr^{3+} spectra in TMFG: (a) S band ($\nu = 3.96$ GHz), PZG glass (1.21 wt% CrF_3), $T = 300$ K; (b) X band ($\nu = 9.43$ GHz), PBI glass (0.20 wt% CrF_3), $T = 4$ K; (c) K band ($\nu = 19.2$ GHz), PBI glass (0.50 wt% CrF_3), $T = 4$ K; (d) Q band ($\nu = 33.88$ GHz), PBI glass (0.50 wt% CrF_3), $T = 300$ K.

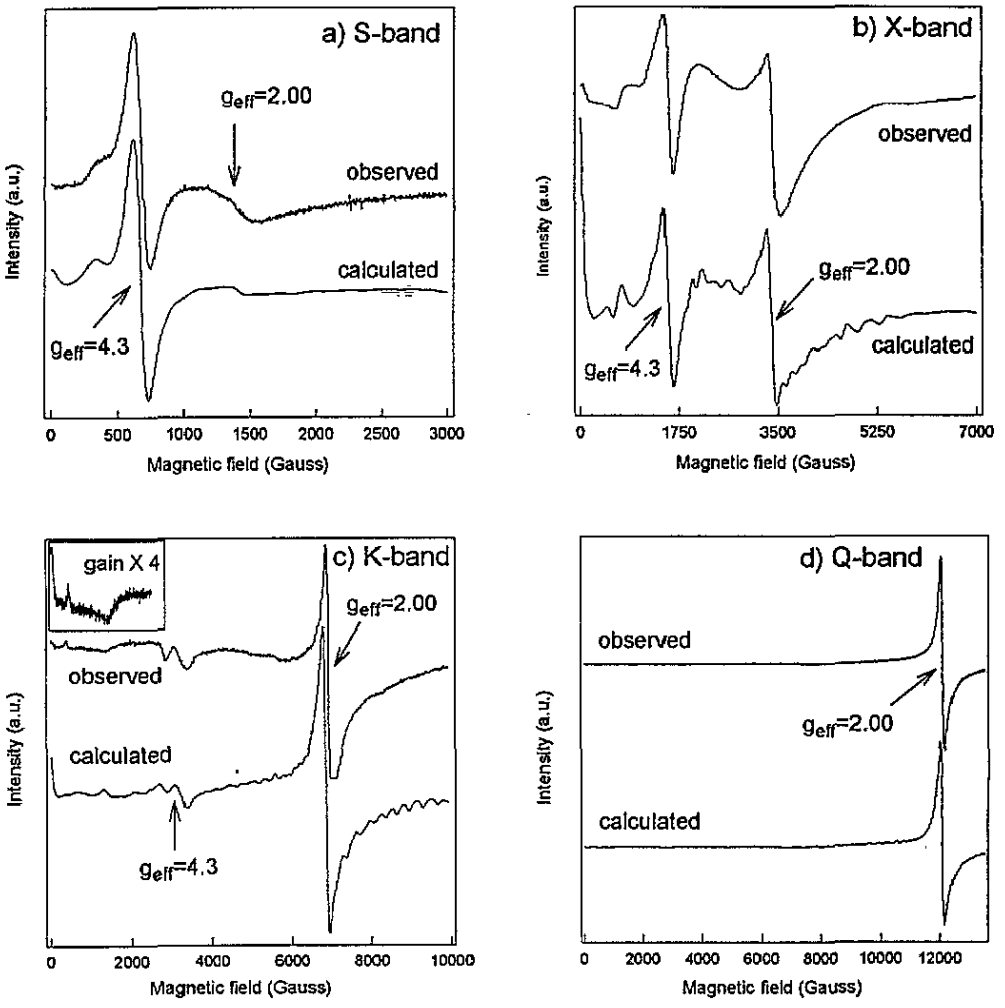

Figure 2. Observed and calculated EPR Fe^{3+} spectra in TMFG. (a) S band ($\nu = 3.96$ GHz), PBI glass (0.50 wt% FeF_3), $T = 300$ K; (b) X band ($\nu = 9.49$ GHz), PBI glass (0.20 wt% FeF_3), $T = 4$ K; (c) K band ($\nu = 19.2$ GHz), PZG glass (0.10 wt% FeF_3), $T = 4$ K; (d) Q band ($\nu = 33.88$ GHz), PZG glass (0.25 wt% FeF_3), $T = 300$ K.

3.3. Discussion

Figure 3 is the absorption spectrum corresponding to the EPR spectrum presented in figure 1(b). It gives evidence for a decrease of the absorption signal near $H = 0$. This phenomenon, which is not fully understood, takes place at low temperature and low probe concentration only. It indicates that absorption occurs for low magnetic field values.

The Cr^{3+} spectra can be described by the spin Hamiltonian

$$H = g\beta \boldsymbol{H} \cdot \boldsymbol{S} + \tfrac{1}{3}(b_2^0 O_2^0 + b_2^2 O_2^2) \qquad (1)$$

where the first term is the electronic Zeeman interaction and the second one is the fine-structure term. The O_n^m expressions are given in table 1 and the other symbols have their usual meaning. The zero-field splitting between the Kramers doublets is given by $\Delta = 2b_2^0(1 + \lambda^2/3)$ with $\lambda = b_2^2/b_2^0$ the asymmetry parameter ($0 \leqslant \lambda \leqslant 1$).

Table 1. U_m, O_n^m and K_n^m expressions (r_n, θ_n, and φ_n are polar coordinates).

O_n^m	U_m	K_n^m
$O_2^0 = 3S_z^2 - S(S+1)$	$U_1 = V_{zz}/2 = \frac{1}{2}\sum q_n(3\cos^2\theta_n - 1)r_n^{-3}$	$K_2^0 = \frac{1}{2}(3\cos^2\theta - 1)$
$O_2^1 = \frac{1}{2}(S_zS_x + S_xS_z)$	$U_2 = V_{xz}/2 = \sqrt{3}\sum_n q_n \sin\theta_n \cos\theta_n \cos\varphi_n\ r_n^{-3}$	$K_2^1 = 3\sin 2\theta \cos\varphi$
$O_2^{-1} = \frac{1}{2}(S_zS_y + S_yS_z)$	$U_3 = V_{yz}/2 = \sqrt{3}\sum_n q_n \sin\theta_n \cos\theta_n \sin\varphi_n\ r_n^{-3}$	$K_2^{-1} = 3\sin 2\theta \sin\varphi$
$O_2^2 = S_x^2 - S_y^2$	$U_4 = V_{xy}/\sqrt{3} = \frac{\sqrt{3}}{2}\sum_n q_n \sin^2\theta_n \sin 2\varphi_n\ r_n^{-3}$	$K_2^2 = \frac{3}{2}\sin^2\theta\cos 2\varphi$
$O_2^{-2} = S_xS_y + S_yS_x$	$U_5 = (V_{xx} - V_{yy})/2\sqrt{3} = \frac{\sqrt{3}}{2}\sum_n q_n \sin^2\theta_n \cos 2\varphi_n\ r_n^{-3}$	$K_2^{-2} = \frac{3}{2}\sin^2\theta\sin 2\varphi$

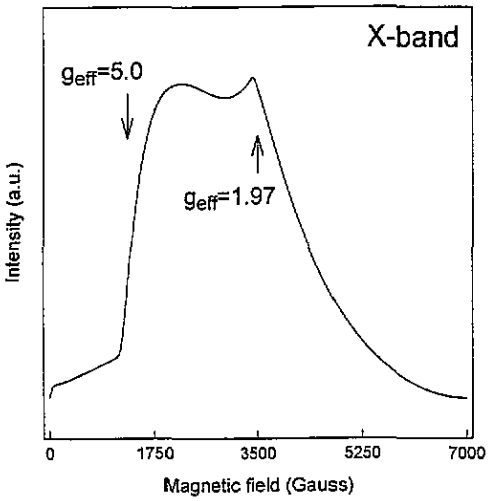

Figure 3. The EPR X band (ν = 9.43 GHz) integrated spectrum of PBI glass:Cr^{3+} (0.20 wt% CrF_3); T = 4 K.

EPR Cr^{3+} spectra were reported in many glasses (phosphates [8, 9], fluorophosphates [9], borosulphates [10], fluoroberyllates [9], fluoroaluminates [11], fluorozirconates [12] and so on). The $g_{eff} = 5.0$ resonance is generally attributed to isolated Cr^{3+} ions in strongly distorted sites, characterized by $\Delta > h\nu$ values. One resonance at $g_{eff} \approx 2.0$ is generally observed and attributed to Cr^{3+} ions pairs [8, 9–11]. The $g_{eff} = 1.97$ resonance, attributed to isolated Cr^{3+} ions, is related to weakly distorted sites, characterized by $\Delta < h\nu$.

The S and Q band studies allow us to find the extreme values for Δ in TMFG: the weak intensity of the $g_{eff} = 1.97$ and the $g_{eff} = 5.0$ resonance at the S and Q bands respectively shows that Cr^{3+} ions are characterized by Δ values between $h\nu_S$ and $h\nu_Q$ ($0.06 < b_2^0$ (cm^{-1}) < 0.55). The observation of signal at both $g_{eff} = 5.0$ and $g_{eff} = 1.97$ in X and K bands implies the presence of sites for which $\Delta > h\nu_K$, $\Delta < h\nu_X$ and $h\nu_X < \Delta < h\nu_K$. The absorption near zero field in these two frequency ranges shows the existence of Cr^{3+} ions for which and $\Delta \approx h\nu_K$ and $\Delta \approx h\nu_X$ ($b_2^0 \approx 0.15$ cm^{-1} and $b_2^0 \approx 0.3$ cm^{-1}). It follows from these results that Cr^{3+} ions are characterized by a continuous fine-structure parameter (b_2^0) distribution in the range 0.06–0.55 cm^{-1}.

The spin Hamiltonian of (1) previously used for Cr^{3+} is generally sufficient (with $S = \frac{5}{2}$) to describe the Fe^{3+} EPR spectrum in glasses. It is well known that the $g_{eff} = 4.3$ feature due to Fe^{3+} in glasses arises from an isotropic transition within one of the three Kramers

doublets resulting from the special situation $\lambda = 1$ and $b_2^0 \gg h\nu$ [13]. This resonance has been observed in many fluoride [11, 12, 14–17] and oxide glasses [18–22]. Usually, a resonance whose intensity depends on both the glass type and the Fe^{3+} concentration is also observed at $g_{eff} = 2.0$ [12, 14–20, 22]. Therefore, some authors attribute it to spin–spin interactions [14, 18, 22] while some others relate it to Fe^{3+} ions characterized by $\Delta < h\nu$ [12, 16, 17]. In TMFG, Fe^{3+} ions contribute to both $g_{eff} = 2.0$ and $g_{eff} = 4.3$ resonances. A similar spectrum was observed in fluorozirconate glass by Griscom and Ginther [17]; they noticed that Fe^{3+} has non-zero EPR absorptions for zero applied magnetic field. They deduced that the simultaneous presence of signal intensity at both zero field and $g_{eff} = 2.0$ in their glass implied respectively the presence of some sites for which $b_2^0 = 0.3h\nu$ and some sites for which $b_2^0 < 0.3h\nu$. In TMFG, the spectrum dependence upon the microwave frequency shows the simultaneous presence of sites for which $b_2^0 > 0.3h\nu$ ($g_{eff} = 4.3$ resonance), $b_2^0 = 0.3h\nu$ and $b_2^0 < 0.3h\nu$ at both X and K bands. The Q and S band spectra indicate that $h\nu_S < \Delta < h\nu_Q$. The continuous Fe^{3+} fine-structure parameter distribution thus ranges between 0.04 and 0.33 cm^{-1} with a maximum around 0.1 cm^{-1}.

4. Cr^{3+} and Fe^{3+} EPR spectra reconstruction

4.1. The Czjzek distribution

Among the various approaches for the $P(b_2^0, \lambda)$ distribution function, we used the one developed by Czjzek [4], considering amorphous solids with random ionic coordination yielding an analytic expression of the distribution of electric field gradient (EFG) $P(V_{zz}, \eta)$. This distribution has already been used for the reconstruction of the EPR Cr^{3+} spectrum in amorphous AlF_3 [23]. The spectrum simulation of TMFG:Fe^{3+} has been briefly presented in a previous paper [24].

4.1.1. The EFG and EPR fine-structure tensor. The use of this distribution is founded on the analogy between the EFG and the fine-structure interaction in EPR tensor component expressions.

The EFG tensor caused by an assembly of discrete charges q_n at a nucleus is symmetric and traceless. It is thus determined by five independent quantities U_m collected in table 1. By a suitable choice of the coordinate system, the tensor **V** only depends on two parameters: V_{zz} and the asymmetry parameter $\eta = (V_{xx} - V_{yy})/V_{zz}$ (with the above convention: $0 \leqslant \eta \leqslant 1$).

The Cr^{3+} ($3d^3$, $S = \frac{3}{2}$) and Fe^{3+} ($3d^5$, $S = \frac{5}{2}$) spin Hamiltonian fine-structure term is

$$H_{sf} = \sum_{n=0}^{2S-1} \sum_{n=-m}^{m} B_n^m O_n^m. \tag{2}$$

By neglecting higher-order terms for Fe^{3+}, it becomes

$$H_{sf} = \tfrac{1}{3}(b_2^0 O_2^0 + b_2^2 O_2^2 + b_2^{-2} O_2^{-2} + b_2^1 O_2^1 + b_2^{-1} O_2^{-1}). \tag{3}$$

The O_n^m expressions are given in table 1.

According to the superposition model introduced by Newman [25], the b_n^m parameters depend on the local surroundings of the paramagnetic ion through the law

$$b_n^m = \sum_i b_n(R_i) K_n^m(\theta_i, \varphi_i) \tag{4}$$

where i runs over the nearest neighbours at coordinates R_i, θ_i and φ_i. $b_n(R_i)$ is a radial function. The $K_n^m(\theta_i, \varphi_i)$ terms are angular functions similar to the angular terms of U_m parameters. For $n = 2$, the $K_n^m(\theta_i, \varphi_i)$ functions are listed table 1.

The fine-structure tensor can be expressed as a 3×3 symmetric traceless matrix. Then, in its eigen-axes, it depends on two parameters: b_2^0 and $\lambda = b_2^2/b_2^0$.

4.1.2. Czjzek's distribution. In amorphous solids, the distribution of the charges q_n leads to an energy level distribution described by a function $P(V_{zz}, \eta)$. This function can be expressed in terms of the $P_m(U_m)$ distribution. In the model developed by Czjzek and coworkers [4],

(i) the EFG is calculated without taking into account the covalence,
(ii) the ions are treated as hard spheres,
(iii) the system is considered as isotropic on average,
(iv) the surroundings of the ion containing the probe nucleus are built up from spherical coordination shells. The structural randomness is defined by a random distribution of ionic angular positions in any shell and by an absence of any correlation between the distributions of ionic charges in different shells.

Under these conditions, $P_m(U_m)$ are Gaussian functions with equal width. Considering the U_m as independent random variables (lack of all geometrical constraints) the distribution function is given by

$$P(V_{zz}, \eta) = \left[1/(2\pi)^{1/2}\sigma^5\right] V_{zz}^4 \eta(1 - \eta^2/9) \exp\left[-V_{zz}^2(1 + \eta^2/3)/2\sigma^2\right]. \quad (5)$$

Fluoride compounds have a pronounced ionic character through the large fluorine electronegativity. Therefore they satisfy the first and the second assumptions used in this model, the third hypothesis is validated by the isotropic character of glasses.

An alteration of the Czjzek distribution function [26] was proposed to take into account geometrical constraints. Indeed, the previous distribution squares with a total disorder (no correlation between atomic positions and consequently between U_m parameters). For instance, it may be easily understood that some local order implies a linear correlation between several of the U_m parameters [27]. Then, the number of degrees of freedom is reduced, leading to the distribution function

$$P(V_{zz}, \eta) = \left[1/(2\pi)^{1/2}\sigma^d\right] V_{zz}^{d-1} \eta(1 - \eta^2/9) \exp\left[-V_{zz}^2(1 + \eta^2/3)/2\sigma^2\right] \quad (6)$$

with $d < 5$.

Taking into account the similarity of the fine-structure Hamiltonian and the nuclear quadrupole interaction Hamiltonian, the determination of a $P(b_2^0, \lambda)$ distribution describing structural disorder around the paramagnetic probes meets Czjzek's model. Then, the $P(b_2^0, \lambda)$ distributions can be written as

$$P(b_2^0, \lambda) = \left[1/(2\pi)^{1/2}\sigma^d\right] (b_2^0)^{d-1} \lambda(1 - \lambda^2/9) \exp\left[-(b_2^0)^2(1 + \lambda^2/3)/2\sigma^2\right]. \quad (7)$$

4.1.3. The distribution function trend and properties: σ and d influence. The function $P(b_2^0, \lambda)$ yields zero probability for both $b_2^0 = 0$ and $\lambda = 0$ (figure 4). These results prohibit the existence of high-symmetry octahedra, which is in agreement with the notion of disorder generally considered in these glasses.

σ and d are two adjustable parameters: σ characterizes the interaction force and d is the number of independent random variables. An increase of d induces a shift of the $P(b_2^0, \lambda)$ maximum to higher b_2^0 values. An increase of σ induces a shift of the $P(b_2^0, \lambda)$ maximum to higher b_2^0 values and a broadening of the distribution.

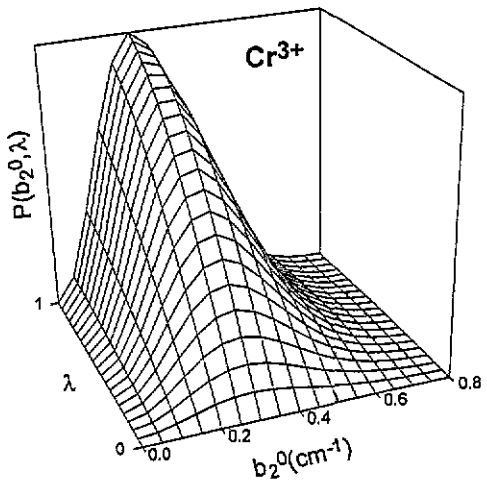

Figure 4. $P(b_2^0, \lambda)$ for $\sigma = 0.21$ cm^{-1} and $d = 3$.

4.2. The computer procedure

The procedure used for the line shape calculation is as follows.

Step I. The 6×6 (Fe^{3+}) or 4×4 (Cr^{3+}) matrix generated from the Hamiltonian (1) is exactly solved for fixed values of b_2^0, b_2^2, θ (the polar angle between $\boldsymbol{H}$ and the z direction of the principal axis system) and φ (the azimuthal angle) and for a choice of external magnetic field values. This gives a set of energy eigenvalues as a function of H.

Step II. The resonant field for each transition is computed by comparing the separation between each pair of energy eigenvalues with the energy of the microwave quantum and by iterating step I until those energy level separations are found that match the microwave quantum.

Step III. Each resonance so found is assigned a derivative linear combination of Gaussian and Lorentzian lines whose amplitude is taken to be proportional to the transition probability: $|\langle i|\boldsymbol{S} \cdot \boldsymbol{B}_{osc}|j\rangle|^2$ where i and j are the two levels from which the transition occurs. $\boldsymbol{S}$ is the spin vector and $\boldsymbol{B}_{osc}$ the oscillating field. The coefficients of the linear combination are adjustable parameters. We calculate the transition width $L = L_0 + \Delta L$: L_0 is the unique isotropic line width and $\Delta L = k(\partial H/\partial\theta)\ \Delta\theta$ where k is an adjustable parameter (the same value for all calculated spectra), which takes into account the line width anisotropy.

Step IV. The calculated spectra for each $\boldsymbol{B}$ orientation are weighted by the factor $dP(\theta, \varphi) = d\Omega(\theta, \varphi)/4\pi$ with $d\Omega(\theta, \varphi) = \sin\theta\, d\theta\, d\varphi$ in accordance with the unit sphere angle dependence on θ.

Step V. A powder-like spectrum is computed by summing the calculated spectra over the orientation angles θ and φ . The glass spectrum is then obtained by summation of these powder-like spectra over the $P(b_2^0, \lambda)$ distribution. The integrations are performed by means of the Gauss–Legendre method.

4.3. Results: σ and d value determination

Appreciable alterations in calculated spectrum trends (change in main resonance intensity ratio) are induced by σ and d variations. The other adjustable parameters (number of poles used for Gauss–Legendre integration, isotropic line width, etc) are not so pertinent as σ and

d. They essentially allow us to reduce the background noise and to improve the resonance trend.

By the trial and error method with integer d values, a simultaneous agreement for Cr^{3+} and Fe^{3+} ions at any frequency is obtained with a single set (σ, d):

$\sigma = 2100(\pm 200) \times 10^{-4}$ cm^{-1}	$d = 3$	for Cr^{3+} (figure 4)
$\sigma = 810(\pm 80) \times 10^{-4}$ cm^{-1}	$d = 3$	for Fe^{3+}.

Calculated spectra are shown in figures 1 (Cr^{3+}) and 2 (Fe^{3+}). The Landé tensor values (considered as isotropic on average), the number of poles (n) used for Gauss–Legendre integration and the isotropic line width are listed below:

Cr^{3+}: $g = 1.97$, $n(b_2^0) = 45$, $n(b_2^2) = 45$, $n(\theta) = 31, n(\varphi) = 31$, $L_0 = 60$ G

Fe^{3+}: $g = 2.002$, $n(b_2^0) = 33$, $n(b_2^2) = 33$, $n(\theta) = 19$, $n(\varphi) = 19$, $L_0 = 80$ G.

A good agreement between observed and calculated spectra is obtained whatever the frequency band.

4.4. Discussion

Although numerous studies have been devoted to Cr^{3+} and Fe^{3+} spectra in amorphous compounds, only two of them have dealt with their reconstructions. The spectrum reconstruction of amorphous AlF_3:Cr^{3+} has been realized using the Czjzek distribution [23]. On the other hand, Fe^{3+} spectra in phosphate and borate glasses have recently been simulated [22] using a fine-structure Gaussian distribution leading to high probability values for $\lambda = 0$ (highly symmetric sites); however, the existence of such sites is quite unlikely in disordered compounds. Simulation of Fe^{3+} spectra in oxide glasses is less favourable than in TMFG as the Fe^{3+} ion coordination is not clearly established yet. Moreover, the use of only one distribution might not be appropriate to simulate the various (tetrahedral, octahedral) coordinations that might coexist in oxide glasses.

The following distribution [26]

$$P(\Delta) = (\Delta^{d-1}/\sigma^d)\exp(-\Delta^2/2\sigma^2) \tag{8}$$

was used for Mössbauer spectra simulation of disordered compounds [28, 29] as this technique allows us to obtain the quadrupolar splitting values $\Delta = V_{zz}\sqrt{1+\eta^2/3}$. This function leads to equal probability values whatever the η values. Nevertheless, a random octahedral structure has been successfully generated by computer [28]. The quadrupolar splitting distribution was in good agreement with the Mössbauer results on amorphous FeF_3. The associated $P(\eta)$ distribution yielded zero probability for $\eta = 0$ in accordance with Czjzek distribution. The d parameter values deduced from the quadrupole splitting distribution were found to be between two and three:

amorphous FeF_3	$d = 2.9$	[28]
amorphous $KFeF_4$	$d = 2$–3	[29]
PMF glass (PbF_2–MnF_2–FeF_3)	$d = 2$	[29]

The d value deduced from Cr^{3+} and Fe^{3+} EPR spectra simulation in TMFG is $d = 3$. This result shows short-range ordering effect involving correlation between b_2^m parameters [27]. In TMFG, disorder is not fully random as the basic structural unit is known (the octahedron): the local order of these octahedra in TMFG might be described by three independent variables: M–F distance, angle between perpendicular bonds ($\approx 90°$) and angle between opposite bonds ($\approx 180°$).

5. Conclusion

We have shown that a single distribution of crystal field parameters, $P(b_2^0, \lambda)$, initially applied by Czjzek to the calculation of electric field gradient in amorphous materials, allows us to take into account the essential features of Cr^{3+} and Fe^{3+} EPR spectra in TMFG and to reconstruct these spectra accurately. The function $P(b_2^0, \lambda)$ yields zero probability for both $b_2^0 = 0$ and $\lambda = 0$. These results prohibit the existence of high-symmetry octahedra, which is in agreement with the notion of disorder generally considered in these glasses.

The superposition model allows us to estimate fine-structure parameters knowing the local structure. Unfortunately, the opposite operation is impossible. Therefore, structural models (atomic coordinate distribution) are essential for extracting a quantitative description of short-range ordering (distance and angle value distributions). In a forthcoming paper, two local structure models will be presented with the aim of characterizing octahedral distortions in TMFG.

Acknowledgment

The authors acknowledge P Simon for recording the Q band spectra.

References

[1] Le Bail A, Jacoboni C and De Pape R 1985 *Mater. Sci. Forum* **6** 441
[2] Boulard B, Jacoboni C and Rousseau M 1989 *J. Solid State Chem.* **80** 17
[3] Legein C, Buzaré J Y and Jacoboni C 1993 *J. Non-Cryst. Solids* **161** 112
[4] Czjzek G, Fink J, Götz F, Schmidt H, Coey J M D, Rebouillat J P and Liénard A 1981 *Phys. Rev.* B **23** 2513
[5] Jacoboni C, Le Bail A and De Pape R 1983 *Glass Technol.* **24** 164
[6] Auriault N, Guery J, Mercier A M, Jacoboni C and De Pape R 1985 *Mater. Res. Bull.* **20** 309
[7] Berlinger W and Müller K A 1977 *Rev. Sci. Instrum.* **48** 1161
[8] Landry R J, Fournier J T and Young C G 1967 *J. Chem. Phys.* **46** 1285
[9] Gan Fuxi, Deng He and Liu Huiming 1982 *J. Non-Cryst. Solids* **52** 135
[10] Srinivaso Rao A, Lakshmana Rao J and and Lakshman S V J 1993 *Solid State Commun.* **85** 529
[11] Dance J M, Videau J J and Portier J 1986 *J. Non-Cryst. Solids* **86** 88
[12] Harris E A 1987 *Phys. Chem. Glasses* **28** 196
[13] Castner T Jr., Newell G S, Holton W C and Slichter C P 1960 *J. Chem. Phys.* **32** 668
[14] Bogomolova L D, Jachkin V A, Krasil'nikova N A, Bogdanov V L, Fedorushkova E B and Khalilev V D 1990 *J. Non- Cryst. Solids* **125** 32
[15] Abdrashitova E I and Petrovskii G T 1967 *Dok. Akad. Nauk SSSR* **175** 1305
[16] Bogomolova L D, Caccavale F, Krasil'nikova N A and Reiman S I 1987 *J. Non-Cryst. Solids* **91** 203
[17] Griscom D L and Ginther R J 1989 *J. Non-Cryst. Solids* **113** 146
[18] Kurkjian C R and Sigety E A 1968 *Phys. Chem. Glasses* **9** 73
[19] Loveridge D and Parke S 1971 *Phys. Chem. Glasses* **12** 19
[20] Nicklin R C, Farach H A and Poole C P Jr 1976 *J. Chem. Phys.* **65** 2998
[21] Dance J M, Darnaudery J P, Baudry H and Monneraye H 1981 *Solid State Commun.* **39** 199
[22] Yahiaoui E, Berger R, Servant Y, Kliava J, Cugunov L and Mednis A 1994 *J. Phys.: Condens. Matter* **6** 9415
Yahiaoui E 1993 *Thesis* University of Bordeaux
[23] Latelli H 1991 *Thesis* University of the Maine
[24] Legein C, Buzaré J Y and Jacoboni C 1995 *J. Non-Cryst. Solids* at press
[25] Newman D J 1971 *Adv. Phys.* **20** 197
[26] Czjzek G 1982 *Phys. Rev.* B **25** 4908
[27] Maurer M and Friedt J M 1986 *Hyperfine Interact.* **27** 135
[28] Greneche J M, Varret F and Teillet J 1988 *J. Physique* **49** 243
[29] Lopez-Herrera M E, Greneche J M and Varret F 1983 *Phys. Rev.* B **28** 4944